$Na_2Ln_2Ti_{3-x}Mn_xO_{10}$ (Ln = Sm, Eu, Gd, and Dy; $0 \leq x \leq 1$): A New Series of Ion-Exchangeable Layered Perovskites Containing B-Site Manganese

Raymond E. Schaak,[†] Dawood Afzal,[‡] Joshua A. Schottenfeld,[†] and Thomas E. Mallouk*,[†]

Department of Chemistry, The Pennsylvania State University, University Park, Pennsylvania 16802, and Department of Chemistry, Truman State University, Kirksville, Missouri 63501

Received August 14, 2001. Revised Manuscript Received October 31, 2001

$Na_2Ln_2Ti_{3-x}Mn_xO_{10}$ (Ln = Sm, Eu, Gd, and Dy; $0 \leq x \leq 1$), a new series of triple-layer Ruddlesden−Popper phases, were synthesized by direct solid-state reaction. The smaller lanthanides enhance manganese solubility in the parent titanate, and an optimized synthetic approach allows $Na_2Ln_2Ti_{3-x}Mn_xO_{10}$ to be stabilized relative to competing single-layer and cubic phases. The X-ray diffraction patterns of $Na_2Ln_2Ti_{3-x}Mn_xO_{10}$ can be indexed on a tetragonal unit cell with a doubled *a* axis. The $Na_2Ln_2Ti_{3-x}Mn_xO_{10}$ phases undergo ion exchange, forming $A_2Ln_2Ti_{3-x}Mn_xO_{10}$ (A = Li, NH_4) by exchange in the molten nitrates. $Na_2Ln_2Ti_{3-x}Mn_xO_{10}$ is also amenable to divalent ion exchange, evidenced by the formation of $A^{II}Gd_2Ti_2MnO_{10}$ (A^{II} = Mg, Ca) by ion exchange in aqueous $MgCl_2$ and $Ca(NO_3)_2$, respectively. Temperature-dependent magnetic susceptibility measurements indicate that the $Na_2Ln_2Ti_{3-x}Mn_xO_{10}$ phases are paramagnetic and suggest the onset of weak magnetic ordering at low temperatures (<10 K).

Introduction

Layered perovskites that belong to the Ruddlesden−Popper family,[1] $A'_2[A_{n-1}B_nO_{3n+1}]$ (A′,A = alkali, alkaline earth, or rare earth; B = transition metal), have attracted considerable attention in recent years due to their interesting magnetic and electronic properties. Ruddlesden−Popper phases, which are intergrowths of the perovskite and rocksalt structures, can accommodate a wide range of B-site cations, including Ti, Nb, Ta, V, Mn, Fe, Co, Ni, Cu, and Ru. Depending on the B-site cation, Ruddlesden−Popper oxides can be metals ($Sr_4V_3O_{9.7}$[2] and $La_4Ni_3O_{10}$[3]), superconductors ($La_{2-x}Ba_xCuO_4$[4] and Sr_2RuO_4[5]), colossal magnetoresistors ($La_{2-2x}Sr_{1+2x}Mn_2O_7$[6]), or catalysts ($K_2La_2Ti_3O_{10}$[7]).

The rocksalt layers of most Ruddlesden−Popper phases contain alkaline earth or rare earth cations. By the decrease of the interlayer charge density, it is possible to synthesize a variety of Ruddlesden−Popper phases containing monovalent interlayer cations[8−13] that can be easily exchanged for other cations[9−11,13−16] or cationic structural units.[17,18] Ion-exchangeable layered perovskites are also interesting precursors to novel three-dimensional perovskites, including A-site defective phases such as $La_{2/3}TiO_3$,[10] $SrNb_{2-x}Ta_xO_6$,[11] and $CaNaTa_3O_9$[13] and nondefective phases such as the A-site ordered perovskite $CaEu_2Ti_3O_9$.[19] Recently, we proposed the idea of a complementary toolbox of reactions for converting layered perovskites into new layered and three-dimensional phases,[20] and it now appears that it

* To whom correspondence should be addressed.
† The Pennsylvania State University.
‡ Truman State University.

(1) (a) Ruddlesden, S. N.; Popper, P. *Acta Crystallogr.* **1957**, *10*, 538; *Acta Cyst.* **1958**, *11*, 54.
(2) Itoh, M.; Shikano, M.; Liang, R.; Kawaji, H.; Nakamura, T. *J. Solid State Chem.* **1990**, *88*, 597.
(3) Zhang, Z.; Greenblatt, M. *J. Solid State Chem.* **1995**, *117*, 236.
(4) Bednorz, J. G.; Müller, K. A. *Z. Phys. B* **1986**, *64*, 189.
(5) Maeno, Y.; Hashimoto, H.; Yoshida, K.; Nishizaki, S.; Fujita, T.; Bednorz, J. G.; Lightenberg, F. *Nature* **1994**, *372*, 532.
(6) (a) Kimura, T.; Tomioka, Y.; Kuwahara, H.; Asamitsu, A.; Tamura, M.; Tokura, Y. *Science* **1996**, *274*, 1698. (b) Moritomo, Y.; Asamitsu, A.; Kuwahara, H.; Tokura, Y. *Nature* **1996**, *380*, 141.
(7) (a) Takata, T.; Furumi, Y.; Shinohara, K.; Tanaka, A.; Hara, M.; Kondo, J. N.; Domen, K. *Chem. Mater.* **1997**, *9*, 1063.
(8) (a) Blasse, G. *J. Inorg. Nucl. Chem.* **1968**, *30*, 656. (b) Byeon, S.-H.; Park, K. *J. Solid State Chem.* **1996**, *121*, 430. (c) Floros, N.; Michel, C.; Hervieu, M.; Raveau, B. *J. Mater. Chem.* **1999**, *9*, 3101.
(9) (a) Richard, M.; Brohan, L.; Tournoux, M. *J. Solid State Chem.* **1994**, *112*, 345. (b) Schaak, R. E.; Mallouk, T. E. *J. Solid State Chem.* **2001**, in press.
(10) Gopalakrishnan, J.; Bhat, V. *Inorg. Chem.* **1987**, *26*, 4301.
(11) Ollivier, P. J.; Mallouk, T. E. *Chem. Mater.* **1998**, *10*, 2585.
(12) Gondrand, M.; Joubert, J.-C. *Rev. Chem. Miner.* **1987**, *24*, 33.
(13) Schaak, R. E.; Mallouk, T. E. *J. Solid State Chem.* **2000**, *155*, 46.
(14) Toda, K.; Watanabe, J.; Sato, M. *Solid State Ionics* **1996**, *90*, 15.
(15) (a) Lalena, J. N.; Cushing, B. L.; Falster, A. U.; Simmons, W. B., Jr.; Seip, C. T.; Carpenter, E. E.; O'Connor, C. J.; Wiley, J. B. *Inorg. Chem.* **1998**, *37*, 4484. (b) Hyeon, K.; Byeon, S. *Chem. Mater.* **1999**, *11*, 352.
(16) Schaak, R. E.; Guidry, E. N.; Mallouk, T. E. *J. Chem. Soc., Chem. Commun.* **2001**, 853.
(17) (a) Kodenkandath, T. A.; Lalena, J. N.; Zhou, W. L.; Carpenter, E. E.; Sangregorio, C.; Falster, A. U.; Simmons, W. B., Jr.; O'Connor, C. J.; Wiley, J. B. *J. Am. Chem. Soc.* **1999**, *121*, 10743. (b) Kodenkandath, T. A.; Kumbhar, A. S.; Zhou, W. L.; Wiley, J. B. *Inorg. Chem.* **2001**, *40*, 710.
(18) Gopalakrishnan, J.; Sivakumar, T.; Ramesha, K.; Thangadurai, V.; Subbanna, G. N. *J. Am. Chem. Soc.* **2000**, *122*, 6237.
(19) Schaak, R. E.; Mallouk, T. E. *J. Am. Chem. Soc.* **2000**, *122*, 2798.
(20) Schaak, R. E.; Mallouk, T. E. *Chem. Mater.*, in press.

10.1021/cm010734q CCC: $22.00
Published on Web 01/04/2002

is possible to retrosynthetically design new perovskites with structural features that are inaccessible thermodynamically.

Most ion-exchangeable layered perovskites contain d^0 cations such as Ti^{4+}, Nb^{5+}, and Ta^{5+} in the B-sites of the perovskite block. A few examples of ion-exchangeable layered perovskites with d^n ($n > 0$) B-site cations exist, including $CsLaSrNb_2M^{II}O_9$ (M^{II} = Cu, Zn),[21] $CsLa_2NbMn_2O_{10}$,[22] $Na_2La_2Ti_{3-x}Ru_xO_{10}$ ($0 \le x \le 1$),[23] and $Na_2Sr_2Nb_2MnO_{10}$.[20] To extend this chemistry to the design of interesting magnetic and electronic phases, it is necessary to first synthesize the appropriate layered precursors. In that regard, we report here the synthesis and magnetic characterization of a new series of ion-exchangeable Ruddlesden−Popper phases, $Na_2Ln_2Ti_{3-x}Mn_xO_{10}$ (Ln = Sm, Eu, Gd, and Dy; $0 \le x \le 1$).

Experimental Section

$Na_2Ln_2Ti_{3-x}Mn_xO_{10}$ (Ln = Sm, Eu, Gd, and Dy; $0 \le x \le 1$) was prepared by heating stoichiometric mixtures of Na_2CO_3, Ln_2O_3, TiO_2, and MnO_2 for 30 min at 1100 °C, followed by 6−12 repeated regrinding/reheating steps until the samples were found to be phase pure, as determined by powder X-ray diffraction. Samples were heated in alumina crucibles in air. A 40% excess of Na_2CO_3 was used to compensate for loss due to volatilization. $Li_2Ln_2Ti_{3-x}Mn_xO_{10}$ and $(NH_4)_2Ln_2Ti_{3-x}Mn_xO_{10}$ were prepared by reacting $Na_2Ln_2Ti_{3-x}Mn_xO_{10}$ with at least a 50-fold excess of molten $LiNO_3$ at 300 °C and molten NH_4NO_3 at 180 °C, respectively, for 6 days. $A^{II}Gd_2Ti_2MnO_{10}$ (A^{II} = Mg, Ca) was prepared by reacting $Na_2Gd_2Ti_2MnO_{10}$ with 1 M aqueous $MgCl_2$ and $Ca(NO_3)_2$, respectively, at 45 °C for 6 days. In all cases, the ion exchange solutions and molten salts were replaced twice to ensure complete exchange.

X-ray diffraction (XRD) patterns were obtained on a Philips X-Pert MPD diffractometer in $\theta-\theta$ geometry using monochromatized Cu Kα (λ = 1.5418 Å) radiation. Lattice parameters were refined by a least-squares method using CELREF.[24] Energy-dispersive X-ray spectroscopy (EDS) was performed on a JEOL-JSM 5400 scanning electron microscope at 30 kV accelerating voltage. EDS data was obtained at the Electron Microscope Facility for the Life Sciences in the Biotechnology Institute at the Pennsylvania State University. Data from at least four acquisitions were averaged to obtain the reported results.

DC magnetic susceptibility measurements were made on a Quantum Design MPMS SQUID magnetometer. Measurements were collected at a field of 1000 Oe, and most samples were analyzed between 2 and 300 K. Both field-cooled (FC) and zero-field-cooled (ZFC) measurements were obtained. There was no detectable difference between the FC and ZFC data, so only the FC data is presented. All measurements were obtained on powder samples placed in gel capsules and secured inside plastic straws.

Results and Discussion

Synthesis of $Na_2Ln_2Ti_{3-x}Mn_xO_{10}$. The synthesis of ion-exchangeable layered perovskites that contain d^n ($n > 1$) B-site cations can be challenging, since many d^n cations have atomic radii, coordination preferences, and distortions (e.g., Jahn−Teller) that differ from their d^0 counterparts. Likewise, there are often competing phases that are more stable than the desired layered perovskite. To successfully incorporate Mn^{4+} into the parent $Na_2Ln_2Ti_3O_{10}$ layered perovskites, we employed two strategies. First, we increased the solubility of Mn^{4+} (which is significantly smaller than Ti^{4+}) in $Na_2Ln_2Ti_3O_{10}$ by incorporating the smaller lanthanides into the perovskite block. Second, we optimized a synthetic approach of iterative brief heating and regrinding that stabilized the target phase relative to the competing kinetically and thermodynamically stable phases.

Since Mn^{4+} (r = 0.530) is smaller than Ti^{4+} (r = 0.605),[25] we envisoned that it should be possible to stabilize Mn^{4+} in the titanate framework by incorporating the smaller lanthanide cations Sm^{3+}, Eu^{3+}, Gd^{3+}, and Dy^{3+} into the A-sites of the perovskite block. Lalena and Wiley were successful in synthesizing $Na_2La_2Ti_{2.2}Mn_{0.8}O_{10}$,[26,27] but we found that it is difficult to reproducibly synthesize phase-pure $Na_2La_2Ti_{3-x}Mn_xO_{10}$ for higher concentrations of manganese. Accordingly, we were able to synthesize $Na_2Gd_2Ti_{2.2}Mn_{0.8}O_{10}$ and found that it was possible to push the solubility of Mn to x = 1 in $Na_2Gd_2Ti_{3-x}Mn_xO_{10}$. Upon exploring the other lanthanides, we found that the largest lanthanide that forms phase-pure $Na_2Ln_2Ti_{3-x}Mn_xO_{10}$ for $x = 1$ is Sm^{3+}. For Ln = Nd, a small amount of a cubic perovskite impurity is unavoidable, and for Ln = La, larger amounts of impurities, which are easily detected by XRD and magnetic susceptibility measurements, are usually observed. (Interestingly, attempts to prepare $Na_2Y_2Ti_{3-x}Mn_xO_{10}$, which contains the smaller Y^{3+} ion, were unsuccessful.)

The x = 1 phases, $Na_2Ln_2Ti_2MnO_{10}$, represent the highest concentration of Mn^{4+} incorporated directly into an ion-exchangeable Ruddlesden−Popper phase to date. Unfortunately, we were not able to extend the solubility of Mn in these compounds to $x > 1$. Also, while we assume that most of the manganese in $Na_2Ln_2Ti_{3-x}Mn_xO_{10}$ is Mn^{4+}, there is most likely some Mn^{3+} present, which would create small numbers of oxygen vacancies in the lattice, as in $Na_2Ln_2Ti_{3-x}Mn_xO_{10-\delta}$. Attempts to determine the oxidation state of Mn by redox titrations failed because none of the $Na_2Ln_2Ti_{3-x}Mn_xO_{10}$ samples could be dissolved. (Several other examples of layered perovskites that do not dissolve, even under harsh conditions, are known.[17,19])

Most ion-exchangeable layered perovskites are synthesized by heating the constituent oxides and carbonates to between 1000 and 1300 °C for 1 or more days. In some cases, the layered phase decomposes into a cubic perovskite upon heating, so obtaining phase-pure materials is sometimes challenging. For example, the single-layer Ruddlesden−Popper phase $NaLnTiO_4$ is best prepared by reacting the appropriate oxides and carbonates at 950 °C for 30 min.[28] $NaLnTiO_4$ is formed initially and can be trapped by the short reaction time, since decomposition to the more stable $Na_2Ln_2Ti_3O_{10}$ occurs over time. Likewise, the triple-layer Ruddles-

(21) Gopalakrishnan, J.; Uma, S.; Vasanthacharya, N. Y.; Subbanna, G. N. *J. Am. Chem. Soc.* **1995**, *117*, 2353.
(22) Takakuwa, S.; Saitoh, T.; Toda, K.; Kanamaru, F. *Key Eng. Mater.* **1999**, *169−170*, 243.
(23) Lalena, J. N.; Falster, A. U.; Simmons, W. B.; Carpenter, E. E.; Wiggins, J.; Hariharan, S.; Wiley, J. B. *Chem. Mater.* **2000**, *12*, 2418.
(24) CELREF (Beta version, Jan 30, 2000) is part of the LMGP Suite for Windows by Jean Laugier and Bernard Bochu.
(25) Six-coordinate radii based on Shannon, R. D. *Acta Crystallogr.* **1976**, *A32*, 751.
(26) Wiley, J. B. Personal communication.
(27) Lalena, J. N. Ph.D. Thesis, University of New Orleans, New Orleans, LA, 1999.
(28) Toda, K.; Kameo, Y.; Kurita, S.; Sato, M. *J. Alloys Compd.* **1996**, *234*, 19.

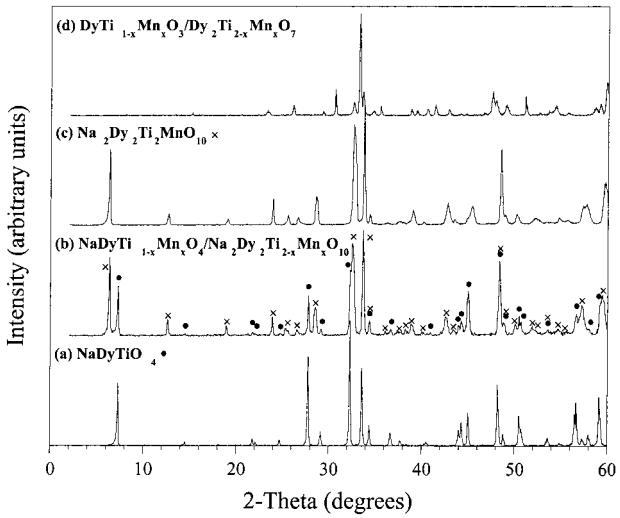

Figure 1. XRD patterns for (a) $NaDyTiO_4$, (b) the mixture of $NaDyTi_{1-x}Mn_xO_4$ and $Na_2Dy_2Ti_{3-x}Mn_xO_{10}$ that is formed initially, (c) phase-pure $Na_2Dy_2Ti_2MnO_{10}$, and (d) the thermodynamically stable products $DyTi_{1-x}Mn_xO_2$ and $Dy_2Ti_{2-x}Mn_xO_7$ that are formed by heating $Na_2Dy_2Ti_2MnO_{10}$ to 1200 °C for 6 h.

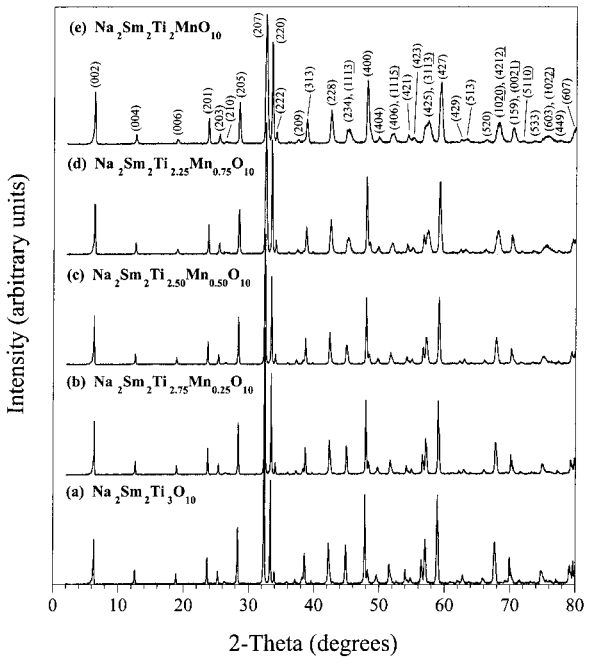

Figure 2. XRD patterns of the $Na_2Sm_2Ti_{3-x}Mn_xO_{10}$ series for (a) $x = 0$, (b) $x = 0.25$, (c) $x = 0.50$, (d) $x = 0.75$, and (e) $x = 1$.

den−Popper phase $K_2Ca_2Ta_2TiO_{10}$ forms only at 1300 °C where decomposition to a cubic phase is unavoidable, but it can be isolated with minimal decomposition by limiting the reaction time to 60 min.[13]

Initial attempts to prepare the triple-layer Ruddlesden−Popper phases $Na_2Ln_2Ti_{3-x}Mn_xO_{10}$ by extended heating at temperatures between 950 and 1300 °C failed because of decomposition to a cubic phase. In contrast, after a 30 min reaction time at 1100 °C, there was no evidence of a cubic impurity; instead, a mixture of the single-layer phase $NaLnTi_{1-x}Mn_xO_4$ and the desired triple-layer phase $Na_2Ln_2Ti_{3-x}Mn_xO_{10}$ was formed (Figure 1b). Every peak in the XRD pattern of $Na_2Dy_2Ti_{3-x}Mn_xO_{10}/NaDyTi_{1-x}Mn_xO_4$, the representative two-phase sample shown in Figure 1b, can be matched to the single-layer phase $NaDyTiO_4$ (Figure 1a) and the triple-layer phase $Na_2Dy_2Ti_2MnO_{10}$ (Figure 1c). When the sample is reground and heated again to 1100 °C for 30 min, the peaks corresponding to the single-layer $NaDyTi_{1-x}Mn_xO_{10}$ phase decrease in intensity while the peaks for the desired $Na_2Dy_2Ti_{3-x}Mn_xO_{10}$ phase increase in intensity. After 6−12 iterations of regrinding/reheating, phase-pure $Na_2Dy_2Ti_2MnO_{10}$ (Figure 1c) is formed with no cubic perovskite impurity. (It is not yet clear why heating at 1100 °C for several hours directly is significantly different from heating for the same length of time in short steps. It is possible that better mixing through intermediate grindings helps to direct the formation of the desired product.)

For comparison purposes, phase-pure $Na_2Dy_2Ti_2MnO_{10}$ from Figure 1c was heated to 1200 °C for 6 h, and the resulting XRD pattern is shown in Figure 1d. (Similar results were obtained by heating phase-pure $Na_2Dy_2Ti_2MnO_{10}$ to 1100 °C for 6 h.) The diffraction pattern in Figure 1d is dominated by a cubic $DyTi_{1-x}Mn_xO_3$ perovskite phase as well as a $Dy_2Ti_{2-x}Mn_xO_7$ pyrochlore phase. (A few peaks from $Na_2Dy_2Ti_2MnO_{10}$ remain in Figure 1d, but they constitute only a small fraction of the sample.) Direct solid-state reactions of stoichiometric amounts of Na_2CO_3, Dy_2O_3, TiO_2, and MnO_2 at 1100 °C for 6 h always produce a cubic perovskite phase as the dominant product, and a diffraction pattern similar to that shown in Figure 1d is obtained.

It is evident from Figure 1 that the single-layer $NaLnTi_{1-x}Mn_xO_4$ phase is formed initially and is the kinetically stabilized product. Upon being further heated, $NaLnTi_{1-x}Mn_xO_4$ is transformed to the triple-layer $Na_2Ln_2Ti_{3-x}Mn_xO_{10}$ phase, which is more stable than the single-layer phase at 1100 °C. Likewise, the cubic perovskite and pyrochlore impurities are the thermodynamically stable products, and they are formed upon extended heating at 1100 °C. Thus, $Na_2Ln_2Ti_{3-x}Mn_xO_{10}$ is an intermediate phase that can be isolated only by carefully controlling the synthesis conditions. Interestingly, the analogous $Na_2Ln_2Ti_3O_{10}$ titanates are sometimes difficult to synthesize as phase-pure materials, and instead they are often prepared by ion exchange of $K_2Ln_2Ti_3O_{10}$. The iterative synthesis approach described here also works for $Na_2Ln_2Ti_3O_{10}$, and it may provide access to new phase-pure layered perovskites in the future.

One possible consequence of the iterative heating approach is that amorphous components, which are not detected by XRD, may be formed. In all cases, scanning electron microscopy (SEM) and transmission electron microscopy (TEM) show well-formed crystallites with no evidence of amorphous components.

Structural Description of $Na_2Ln_2Ti_{3-x}Mn_xO_{10}$. The XRD patterns for the $Na_2Sm_2Ti_{3-x}Mn_xO_{10}$ series are shown in Figure 2, and the lattice parameters for these and the other $Na_2Ln_2Ti_{3-x}Mn_xO_{10}$ phases are presented in Table 1. All of the peaks in the diffraction patterns index to a large tetragonal unit cell that accommodates the staggered perovskite blocks. Interestingly, it was necessary to double the *a* axis lattice parameter to account for all of the reflections. For example, the weak (210) reflection near 26.3° 2θ is present in all of the $Na_2Ln_2Ti_{3-x}Mn_xO_{10}$ phases (including $x = 0$), and it cannot be indexed with the use of a standard unit cell.

Table 1. Lattice Parameter Data for $Na_2Ln_2Ti_{3-x}Mn_xO_{10}$ (Ln = Sm, Eu, Gd, and Dy; $0 \leq x \leq 1$) and $A_2Ln_2Ti_2MnO_{10}$ (A = Li, NH_4)[a]

compound	*a* (Å)	*c* (Å)
$Na_2Sm_2Ti_3O_{10}$	7.6139(2)	28.213(1)
$Na_2Sm_2Ti_{2.75}Mn_{0.25}O_{10}$	7.5978(2)	28.141(1)
$Na_2Sm_2Ti_{2.50}Mn_{0.50}O_{10}$	7.5904(2)	28.245(1)
$Na_2Sm_2Ti_{2.25}Mn_{0.75}O_{10}$	7.5827(3)	28.088(1)
$Na_2Sm_2Ti_2MnO_{10}$	7.5779(4)	28.115(1)
$Na_2Eu_2Ti_3O_{10}$	7.6003(2)	28.304(1)
$Na_2Eu_2Ti_{2.75}Mn_{0.25}O_{10}$	7.5760(4)	28.185(1)
$Na_2Eu_2Ti_{2.50}Mn_{0.50}O_{10}$	7.5685(3)	28.215(1)
$Na_2Eu_2Ti_{2.25}Mn_{0.75}O_{10}$	7.5718(3)	27.942(1)
$Na_2Eu_2Ti_2MnO_{10}$	7.5612(4)	28.053(2)
$Na_2Gd_2Ti_3O_{10}$	7.5789(2)	28.275(1)
$Na_2Gd_2Ti_{2.75}Mn_{0.25}O_{10}$	7.5706(3)	28.277(1)
$Na_2Gd_2Ti_{2.50}Mn_{0.50}O_{10}$	7.5513(3)	28.130(1)
$Na_2Gd_2Ti_{2.25}Mn_{0.75}O_{10}$	7.5315(5)	28.131(2)
$Na_2Gd_2Ti_2MnO_{10}$	7.5245(3)	27.836(1)
$Na_2Dy_2Ti_3O_{10}$	7.5438(2)	28.291(1)
$Na_2Dy_2Ti_{2.75}Mn_{0.25}O_{10}$	7.5363(4)	28.181(1)
$Na_2Dy_2Ti_{2.50}Mn_{0.50}O_{10}$	7.5285(4)	28.073(2)
$Na_2Dy_2Ti_{2.25}Mn_{0.75}O_{10}$	7.5256(3)	27.990(1)
$Na_2Dy_2Ti_2MnO_{10}$	7.5098(3)	27.981(1)
$Li_2Sm_2Ti_2MnO_{10}$	7.5978(5)	25.964(2)
$Li_2Eu_2Ti_2MnO_{10}$	7.5879(4)	26.008(1)
$Li_2Gd_2Ti_2MnO_{10}$	7.5498(3)	26.261(2)
$Li_2Dy_2Ti_2MnO_{10}$	7.5194(2)	26.115(1)
$(NH_4)_2Sm_2Ti_2MnO_{10}$	7.5715(4)	26.356(1)
$(NH_4)_2Eu_2Ti_2MnO_{10}$	7.5637(3)	26.316(1)
$(NH_4)_2Gd_2Ti_2MnO_{10}$	7.5324(7)	26.153(1)
$(NH_4)_2Dy_2Ti_2MnO_{10}$	7.5184(4)	26.727(3)

[a] Standard deviations are given in parentheses.

Identical unit cell doubling was reported previously for $Na_2Gd_2Ti_3O_{10}$,[12] and all of the $Na_2Ln_2Ti_{3-x}Mn_xO_{10}$ phases appear to be isostructural with $Na_2Gd_2Ti_3O_{10}$.

The doubled *a* axis lattice parameter is most likely due to cooperative tilting of the $MO_{6/2}$ octahedra, which forms a superlattice. Unfortunately, we were not able to determine a reliable and consistent structural model for $Na_2Ln_2Ti_{3-x}Mn_xO_{10}$ due to the quality of the laboratory XRD data and the complexity of the large unit cell. It would not have been possible to unambiguously determine the positions of the oxygen atoms in the unit cell, which is crucial to solving the superlattice structure. In addition, it is impossible to distinguish Mn from Ti using XRD, so cation ordering effects such as those found in $Na_2La_2Ti_{3-x}Ru_xO_{10}$ could not be elucidated.[23] Many other Ruddlesden−Popper phases, including the related compounds $Ca_4Mn_3O_{10}$[29] and $Ca_4Mn_2TiO_{9.93}$,[30] have octahedra that cooperatively tilt to form a superlattice that can be indexed to an orthorhombic unit cell with a 2×2 supercell. Attempts to refine the structure of $Na_2Ln_2Ti_{3-x}Mn_xO_{10}$ with a similar model were unsuccessful.

The diffraction patterns for the $x = 0$, 0.25, 0.50, 0.75, and 1.00 members of the $Na_2Sm_2Ti_{3-x}Mn_xO_{10}$ series in Figure 2 show some interesting features. (All of the other $Na_2Ln_2Ti_{3-x}Mn_xO_{10}$ solid solutions are similar.) First, the number of peaks and their positions are nearly identical in all of the diffraction patterns, which suggests that all of the members of the solid solution are isostructural. Also, there are no peaks between 32.7 and 33.0° 2θ, which indicates that there are no cubic perovskite impurities (see Figure 1d for comparison) and that the $Na_2Sm_2Ti_{3-x}Mn_xO_{10}$ compounds are phase pure. Finally, the peaks broaden considerably as more manganese is incorporated into the lattice. SEM images indicate that all of the phases have well-formed crystallites that range in size from 500 nm to 10 μm, which is typical for layered perovskites and indicates that the peak broadening is not caused by particle size effects. Instead, the domain sizes may be smaller as more manganese is incorporated into the lattice, or there could be some structural distortions that arise from the random distribution of the smaller Mn^{4+} cation into the $TiO_{6/2}$ lattice.

The lattice parameter data presented in Table 1, in general, show the trends expected for the incorporation the smaller Mn^{4+} cation into the $TiO_{6/2}$ lattice, although a few exceptions are notable. All of the *a* axis lattice parameters for Ln = Sm and Dy decrease nearly monotonically as more manganese is incorporated into the lattice. For Ln = Eu, the $x = 0.75$ member has an *a* axis lattice parameter that is larger than both the $x = 0.50$ and $x = 1.00$ members, but the *c* axis lattice parameter decreases to compensate. For Ln = Gd, the *a* and *c* axes lattice parameters for the $x = 0.50$ and $x = 0.75$ members are nearly identical. The *c* axis lattice parameters for Ln = Gd and Dy decrease as the manganese concentration increases. For the larger lanthanides (Ln = Sm and Eu), the *c* axis lattice parameters have less periodic variation, although the apparently anomalous increases in the *c* axis lattice parameters in the $x = 0.50$ phases, for example, are usually offset by a decrease in the *a* axis lattice parameter. Apparently, the *a* and *c* axes expand and contract differently among the $Na_2Ln_2Ti_{3-x}Mn_xO_{10}$ solid solution members to accommodate the manganese.

Further evidence for the quantitative incorporation of manganese into $Na_2Ln_2Ti_{3-x}Mn_xO_{10}$ comes from EDS data. Since the Gd L and Eu L lines overlap with the Mn K line, it was only possible to analyze the Ln = Sm and Dy samples. Normalizing to Sm, we found that the Ti/Mn ratios were 3.04:0.00, 2.76:0.23, 2.46:0.53, 2.26:0.74, and 2.00:0.96 for the $x = 0$, 0.25, 0.50, 0.75, and 1.00 samples, respectively. Likewise, the Dy/Ti/Mn ratios in $Na_2Dy_2Ti_2MnO_{10}$ and $Na_2Dy_2Ti_{2.5}Mn_{0.5}O_{10}$ were 2.00:2.00:0.97 and 2.00:2.49:0.54, respectively. (Similar results, accurate to within 10%, were obtained on analyses of multiple batches of the same compositions.) The stoichiometries derived from EDS analysis agree well with those calculated based on the starting ratios, within experimental error.

The EDS analysis was performed both on bulk material and on smaller sets of crystallites. In all cases, the Ti/Mn ratios appeared homogeneous across the samples. Without EDS analysis of individual crystallites, however, we cannot rule out the possibility that the Mn content varies among the crystallites. Such variation would help to explain the discrepancies in the lattice parameters as well as the peak broadening at higher Mn concentrations.

Ion Exchange of $Na_2Ln_2Ti_{3-x}Mn_xO_{10}$. Like the analogous titanates, all of the $Na_2Ln_2Ti_{3-x}Mn_xO_{10}$ phases undergo monovalent ion exchange. The interlayer sodium cations can be replaced by lithium in molten

(29) Battle, P. D.; Green, M. A.; Lago, J.; Millburn, J. E.; Rosseinsky, M. J.; Ventre, J. F. *Chem. Mater.* **1998**, *10*, 658−664.
(30) Battle, P. D.; Blundell, S. J.; Coldea, A. I.; Cussen, E. J.; Rosseinsky, M. J.; Singelton, J.; Spring, L. E.; Vente, J. F. *J. Mater. Chem.* **2001**, *11*, 160.

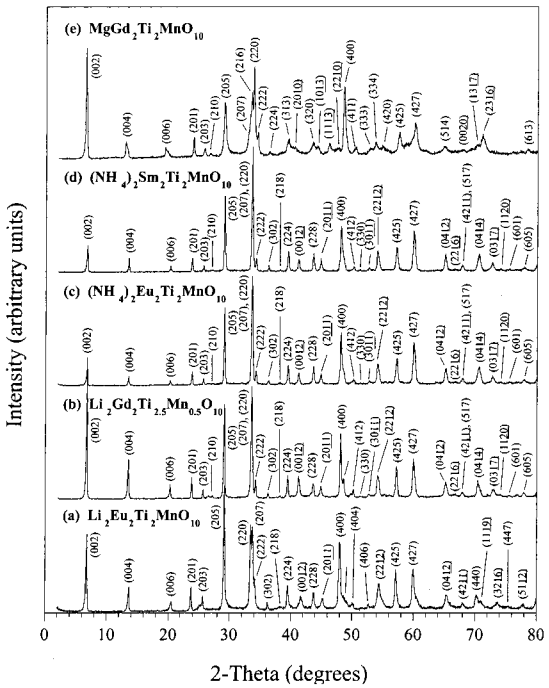

Figure 3. XRD patterns for the ion exchange products: (a) $Li_2Eu_2Ti_2MnO_{10}$, (b) $Li_2Gd_2Ti_{2.5}Mn_{0.5}O_{10}$, (c) $(NH_4)_2Eu_2Ti_2MnO_{10}$, (d) $(NH_4)_2Sm_2Ti_2MnO_{10}$, and (e) $MgGd_2Ti_2MnO_{10}$.

$LiNO_3$ or by ammonium in molten NH_4NO_3. The ion-exchanged phases retain the staggered perovskite sheets and the doubled *a* axis lattice parameters of the parent $Na_2Ln_2Ti_{3-x}Mn_xO_{10}$ phases, and ion exchange is accompanied by a significant contraction of the *c* axis (Table 1). (Nitrogen analysis of the nominal $(NH_4)_2Ln_2Ti_{3-x}Mn_xO_{10}$ phases indicates substoichiometric ion exchange, with the average formula $(NH_4)_{1.25}H_{0.75}Ln_2Ti_{3-x}Mn_xO_{10}$.) Figure 3 shows the XRD patterns for representative ion-exchanged phases. All of the $A_2Ln_2Ti_{3-x}Mn_xO_{10}$ (A = Li, NH_4) phases remain highly crystalline, and all of the reflections can be indexed to an expanded tetragonal unit cell.

Interestingly, we found that $Na_2Ln_2Ti_{3-x}Mn_xO_{10}$ is also amenable to divalent ion exchange, much like $A_2Ln_2Ti_3O_{10}$[15,18,19] and $NaLnTiO_4$.[16,31] As an example, we prepared $MgGd_2Ti_2MnO_{10}$ by the exchange of two Na^+ cations for one Mg^{2+} cation in aqueous $MgCl_2$ (Figure 3e). $MgGd_2Ti_2MnO_{10}$ indexes to a tetragonal unit cell with $a = 7.4873(6)$ and $c = 27.636(2)$, which is significantly contracted along the *a* axis but only slightly contracted along the *c* axis, relative to $Na_2Gd_2Ti_2MnO_{10}$. Interestingly, $MgGd_2Ti_2MnO_{10}$ retains the staggered geometry of its parent phase. In contrast, most other aqueous divalent ion exchange reactions result in a shift of the perovskite slabs to an eclipsed geometry.[16,19] EDS analysis indicates that approximately 18% of the sodium remains in $A^{II}_{x/2}Na_{2-x}Ln_2Ti_{3-x}Mn_xO_{10}$ (A^{II} = Mg, Ca), which could prevent the structural phase transition to eclipsed geometry that is expected upon complete divalent ion exchange. Also, the peaks in the diffraction pattern of $MgGd_2Ti_2MnO_{10}$ are broadened relative to $A_2Ln_2Ti_{3-x}Mn_xO_{10}$ (A = Na, Li, NH_4), which most likely indicates structural disorder along the interlayer gallery. The small Mg^{2+} cations between the perovskite sheets are likely to increase the degree of octahedral tilt in a nonuniform manner, which disrupts some of the long-range periodicity of the structure. $CaGd_2Ti_2MnO_{10}$ can also be formed by divalent ion exchange in aqueous $Ca(NO_3)_2$.

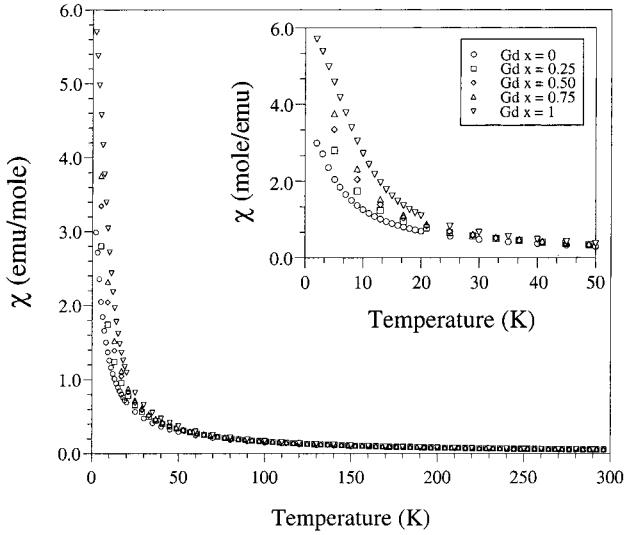

Figure 4. Temperature dependence of the molar magnetic susceptibility (FC) for $Na_2Gd_2Ti_{3-x}Mn_xO_{10}$ (x = 0, 0.25, 0.50, 0.75, and 1.00) at 1000 Oe. The inset shows the expanded temperature region from 2 to 50 K.

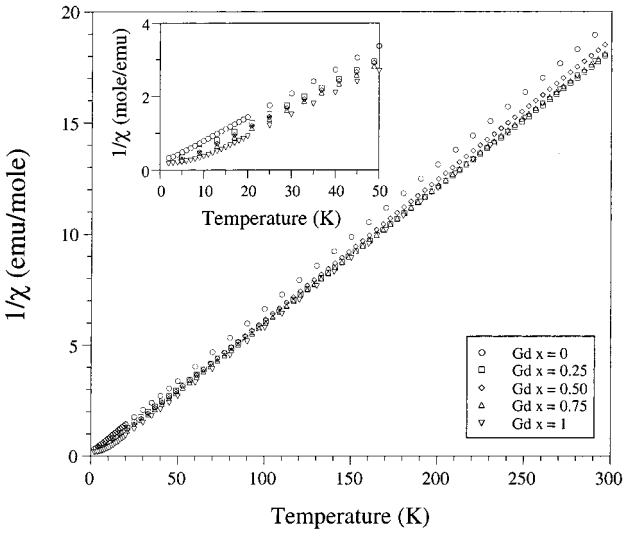

Figure 5. Inverse susceptibility plots for $Na_2Gd_2Ti_{3-x}Mn_xO_{10}$ (x = 0, 0.25, 0.50, 0.75, and 1.00). The inset shows the expanded temperature region from 2 to 50 K.

Magnetic Characterization of $Na_2Ln_2Ti_{3-x}Mn_xO_{10}$. The temperature-dependent molar magnetic susceptibility data for the Ln = Gd series are shown in Figures 4 and 5. The plot of χ vs T in Figure 4 suggests that the $Na_2Gd_2Ti_{3-x}Mn_xO_{10}$ phases are paramagnetic. The inset in Figure 4 shows that the low-temperature magnetic susceptibilities increase as the manganese content increases, although the susceptibilities at higher temperatures are nearly identical for the samples that contain manganese ($x > 0$). The plot of $1/\chi$ vs T in Figure 5 shows that all of the $Na_2Gd_2Ti_{3-x}Mn_xO_{10}$ samples obey the Curie−Weiss law at high temperatures. Deviation from ideal Curie−Weiss behavior occurs around 2 K for

(31) McIntyre, R. A.; Falster, A. U.; Li, S.; Simmons, W. B., Jr.; O'Connor, C. J.; Wiley, J. B. *J. Am. Chem. Soc.* **1998**, *120*, 217.

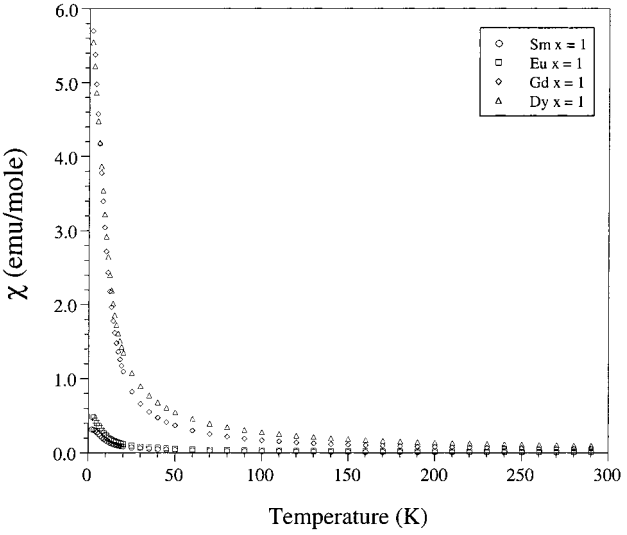

Figure 6. Temperature dependence of the molar magnetic susceptibility (FC) for $Na_2Ln_2Ti_2MnO_{10}$ (Ln = Sm, Eu, Gd, and Dy).

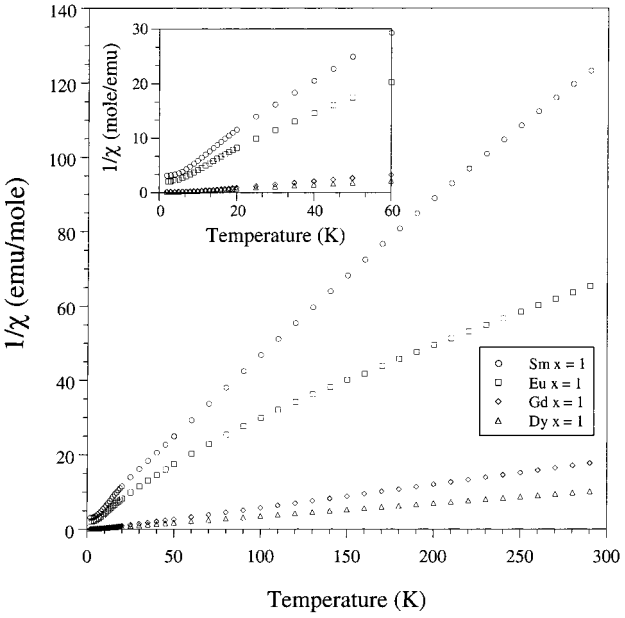

Figure 7. Inverse susceptibility plots for $Na_2Ln_2Ti_2MnO_{10}$. The inset shows the expanded temperature region from 2 to 60 K.

$Na_2Gd_2Ti_3O_{10}$ and around 25 K for $Na_2Gd_2Ti_2MnO_{10}$. Interestingly, $\theta = -2$ K for the $x = 0$ phase, which suggests weak antiferromagnetic ordering at low temperatures, similar to other lanthanide titanates such as $Pr_{2/3}TiO_3$.[32] In contrast, the $x > 0$ samples have positive values of θ ($\theta_{x=0.25} = 2$ K, $\theta_{x=0.50} = 7$ K, $\theta_{x=0.75} = 8$ K, $\theta_{x=1} = 10$ K).[33] The Curie temperature increases with increasing manganese concentration, which suggests that T_c could be increased if more manganese could be incorporated into the perovskite block.

The fact that most of the $Na_2Gd_2Ti_{3-x}Mn_xO_{10}$ samples overlap in Figures 4 and 5 suggests that the magnetic susceptibilities are dominated by the lanthanide cations, which is reasonable considering the large moment of the free Gd^{3+} ion ($\mu_{eff} = 7.94$).[34] The effective localized moment was calculated to be 7.83 μ_B per Gd^{3+} ion in $Na_2Gd_2Ti_3O_{10}$, which is consistent with the expected value. Only small increases in the magnetic moments were observed for the manganese-containing samples.

A plot of χ vs T for $Na_2Ln_2Ti_2MnO_{10}$ (Ln = Sm, Eu, Gd, and Dy) is shown in Figure 6. The Ln = Gd and Dy samples have considerably higher susceptibilities than those for the Ln = Sm and Eu phases, which is consistent with the higher effective moments of the free Gd^{3+} ($\mu_{eff} = 7.94$) and Dy^{3+} ($\mu_{eff} = 10.63$) ions relative to Sm^{3+} ($\mu_{eff,calc} = 0.84$, $\mu_{eff,exp} = 1.5$) and Eu^{3+} ($\mu_{eff,calc} = 0$, $\mu_{eff,exp} = 3.4$).[34]

The Curie plots shown in Figure 7 highlight the subtle differences among the lanthanide samples. $Na_2Dy_2Ti_2MnO_{10}$ appears similar to $Na_2Gd_2Ti_2MnO_{10}$, although $\theta = 0$ for $Na_2Dy_2Ti_2MnO_{10}$. Deviation from Curie−Weiss behavior for $Na_2Dy_2Ti_2MnO_{10}$ occurs around 20 K. $Na_2Eu_2Ti_2MnO_{10}$ can be fit to the Curie−Weiss law only above 150 K, and the slope of the $1/\chi$ vs T plot suggests weak antiferromagnetic ordering at a Weiss temperature of −72 K. $Na_2Sm_2Ti_2MnO_{10}$ exhibits similar behavior, with $\theta = -38$ K. (Similar shifts from ferromagnetic to antiferromagnetic ordering as a function of the lanthanide in titanate perovskites have been observed previously.[32]) The effective magnetic moments obtained from the Curie−Weiss fits decrease according to the trend expected for the free Ln^{3+} ions ($\mu_{eff,Ln=Dy} = 15.06$, $\mu_{eff,Ln=Gd} = 11.22$, $\mu_{eff,Ln=Eu} = 5.87$, and $\mu_{eff,Ln=Sm} = 4.32$ μ_B), but they differ somewhat from those predicted for the free ions. Similar inconsistencies have been observed in other highly distorted Ruddlesden−Popper manganates, including $Ca_4Mn_3O_{10}$.[29]

While we have attempted to choose representative samples for initial magnetic characterization, more complete and detailed studies to fully characterize all of the $Na_2Ln_2Ti_{3-x}Mn_xO_{10}$ phases are in progress, including measurements of the complete magnetic hysteresis loops and measurements of the temperature-dependent resistivity.[35]

Conclusions

In this paper, we have reported the first direct synthesis of ion-exchangeable Ruddlesden−Popper phases that have up to one-third of the B-sites filled with manganese. By the use of the smaller lanthanides Sm^{3+}, Eu^{3+}, Gd^{3+}, and Dy^{3+} in the A-sites of the perovskite block, it was possible to incorporate the smaller manganese cation in the parent titanate framework. Additionally, the optimized synthetic approach allowed $Na_2Ln_2Ti_{3-x}Mn_xO_{10}$ to be stabilized relative to competing single-layer and cubic phases. These approaches could possibly be used to incorporate other interesting magnetic or electronic cations, such as Cr^{3+}, Fe^{3+}, Co^{3+}, or Ni^{3+}, or smaller d^0 cations, such as W^{6+}, Mo^{6+}, or V^{5+}, into ion-exchangeable layered perovskites.

Since $Na_2Ln_2Ti_{3-x}Mn_xO_{10}$ is amenable to ion exchange, it may be possible to transform these layered

(32) Yoshii, K. *J. Solid State Chem.* **2000**, *149*, 354.

(33) Curie temperatures were determined by extrapolating the linear fit to the high-temperature (>150 K) data. Temperature-independent paramagnetic contributions were not considered.

(34) Kittel, C. In *Introduction to Solid State Physics*, 7th ed.; John Wiley: New York, 1996.

(35) Preliminary two-point resistance measurements suggest that all of the $Na_2Ln_2Ti_{3-x}Mn_xO_{10}$ samples are insulators ($R > 32$ MΩ) at room temperature.

perovskites into new layered and three-dimensional perovskites by means of topochemical reactions. For example, the Mn^{4+} layered perovskite $MgGd_2Ti_2MnO_{10}$ could undergo reduction to $MgGd_2Ti_2Mn^{II}O_9$ in a reaction analogous to the topochemical synthesis of the A-site ordered perovskite $CaEu_2Ti_3O_9$.[19] Ion exchange of cationic structural units, such as $Bi_2O_2^{2+}$,[18] could lead to interesting magnetic intergrowth structures. Likewise, ion exchange and reductive intercalation of $Mg_{y/2}Na_{2-y}Ln_2Ti_{3-x}Mn_xO_{10}$ could be used to fine-tune the oxidation state of Mn in a multistep sequence of reactions similar to that used in the synthesis of $Na_{1-x+y}Ca_{x/2}LaTiO_4$.[31] Also, since ion-exchangeable layered perovskites are known to exfoliate into nanoscale colloids,[36] it may be possible to use these new phases as precursors for the assembly of thin film magnetic heterostructures.

Acknowledgment. This work was supported by National Science Foundation Grant CHE-0095394. The authors thank Iosif-Grigore Deac, Joe Snyder, and Peter Schiffer for help in obtaining the magnetic measurements. R.E.S. thanks John Wiley for sharing references and results prior to publication. D.A. thanks the NSF-ROA program (Grant CHE-9529202) for support of his work at Penn State. R.E.S. thanks the National Science Foundation for support in the form of a Graduate Research Fellowship.

CM010734Q

(36) (a) Fang, M.; Kim, H.-N.; Saupe, G. B.; Miwa, T.; Fujishima, A.; Mallouk, T. E. *Chem. Mater.* **1999**, *11*, 1526. (b) Schaak, R. E.; Mallouk, T. E. *Chem. Mater.* **2000**, *12*, 2513. (c) Schaak, R. E.; Mallouk, T. E. *Chem. Mater.* **2000**, *12*, 3427.